Anderson Localization and the Quantum Phase Diagram of Three Dimensional Disordered Dirac Semimetals

J. H. Pixley, Pallab Goswami, and S. Das Sarma

Condensed Matter Theory Center and Joint Quantum Institute, Department of Physics, University of Maryland, College Park, Maryland 20742-4111 USA

We study the quantum phase diagram of a three dimensional noninteracting Dirac semimetal in the presence of either quenched axial or scalar potential disorder, by calculating the average and the typical density of states as well as the inverse participation ratio using numerically exact methods. We show that as a function of the disorder strength a half-filled (i.e., undoped) Dirac semimetal displays three distinct ground states, namely an incompressible semimetal, a compressible diffusive metal, and a localized Anderson insulator, in stark contrast to a conventional dirty metal that only supports the latter two phases. We establish the existence of two distinct quantum critical points, which respectively govern the semimetal-metal and the metal-insulator quantum phase transitions and also reveal their underlying multifractal nature. Away from half-filling the (doped) system behaves as a diffusive metal that can undergo Anderson localization only, which is shown by determining the mobility edge and the phase diagram in terms of energy and disorder.

The development of Lorentz invariant relativistic quantum mechanics naturally led to the discovery of the celebrated Dirac equation [1] to describe the electron and positron. In high energy physics there are no massless Dirac fermions, as both leptons and quarks are massive particles and it is only at energy scales higher than the corresponding mass gap, that they can be approximated as massless. In contrast, many condensed matter systems support a gapless phase, where twofold Kramers degenerate conduction and valence bands touch linearly at isolated points in the Brillouin zone. The low energy excitations around these diabolic points (known as Dirac points, where the conical conduction and valence bands touch each other) can be described by a massless Dirac equation in the infrared limit; such a phase is known as a Dirac semimetal (DSM) if the system is undoped with the Fermi level precisely at the Dirac point.

Recently, an intense experimental investigation into narrow gap semiconductors [2] has led to the discovery of three dimensional DSMs in various materials such as Cd_3As_2 [3–5], Na_3Bi [4,6], $Bi_{1-x}Sb_x$ [7–9], $BiTl(S_{1-\delta}Se_\delta)_2$ [10,11], $(Bi_{1-x}In_x)_2Se_3$ [12,13], and $Pb_{1-x}Sn_xTe$ [2,14,15]. These experiments have now raised the exciting prospect of studying the physics of three dimensional massless Dirac fermions in solid state systems. Because of the ubiquitous presence of disorder in all solid state systems, a precise understanding of the phase diagram of dirty DSMs is therefore a problem of deep fundamental importance, which can only be studied in condensed matter systems since the corresponding relativistic Dirac problem in particle physics does not, by definition, have any disorder. While effects of disorder in conventional metals are fairly

well understood [16–19], this is not the case for three dimensional DSMs where the applicable quantum phase diagram and (even) the question of how many allowed phases may exist as a function of disorder are still wide open.

Because of the finite density of states (DOS) at the Fermi energy, a conventional metal (CM) (or a Fermi liquid) is a compressible state of matter, and an infinitesimally weak disorder acts as a relevant perturbation for the ballistic Fermi liquid fixed point, giving rise to a finite lifetime for the ballistic single particle excitations [20]. Therefore, a dirty, noninteracting CM in three dimensions only supports two phases, namely, a diffusive metal and a localized Anderson insulator (AI) [21]. The Anderson localization is a continuous quantum phase transition (QPT), for which the spatial dimension $d = 2$ serves as the lower critical dimension [21]. This QPT is reflected in the spatial variation of the wave function and can only be captured by quantities that probe its extended or localized nature, such as the inverse participation ratio (IPR) [22,23], and the typical DOS (TDOS) [18,24,25]. However, a self-averaging quantity such as the average DOS (ADOS) itself remains unaffected by the localization transition.

In contrast to CMs, a half-filled (i.e., undoped) three dimensional DSM is an incompressible fermionic quantum critical system, which leads to a quadratically vanishing DOS at the Fermi level. Consequently, any weak disorder acts as an irrelevant perturbation for a three dimensional DSM. Therefore, the three dimensional ballistic DSM phase should remain stable up to a critical strength of disorder W_c. At this threshold, the DSM undergoes a continuous QPT into a compressible diffusive metal

(CDM) phase [26,27], and the ADOS at zero energy acts as an order parameter for describing this transition, while distinguishing it from a conventional Anderson localization. Based on a nonlinear sigma model analysis, the CDM phase has been argued to display an Anderson localization at a higher strength of disorder W_l, which belongs to the unitary (A) universality class [26]. The first analysis of the DSM-CDM transition in Ref. [26] was a mean-field one, and only recently the non-Gaussian nature of this quantum critical point (QCP) has been elucidated [27]. Subsequently, the DSM-CDM phase transition has been addressed using various analytic [28–31] and numerical methods [32–34]. However, the effects of large disorder and the Anderson localization transition have not been studied through any numerically exact approach. Moreover, there have been recent claims that rare-region effects convert the DSM into a CDM for an infinitesimally weak disorder strength [35] so that there is in fact no DSM-CDM transition at all. Therefore, it is still an important open question to figure out how many distinct quantum phases indeed exist in a dirty 3D Dirac system for finite disorder (one or two or three with DSM/CDM/AI being all the possibilities) through a nonperturbative calculation, in addition to establishing the appropriate universality of any applicable disorder-driven QPT in the system. In the current paper we answer this question through extensive exact numerical work supplemented by theoretical arguments.

We study the phase diagram of a dirty DSM in three dimensions using numerically exact methods. We calculate the ADOS and the TDOS on sufficiently large lattice sizes reaching up to 60^3 sites, using the kernel polynomial method (KPM) [36]. As the TDOS tracks the ADOS in any metallic phase and also serves as an order parameter for Anderson localization [18,24], it can naturally capture both
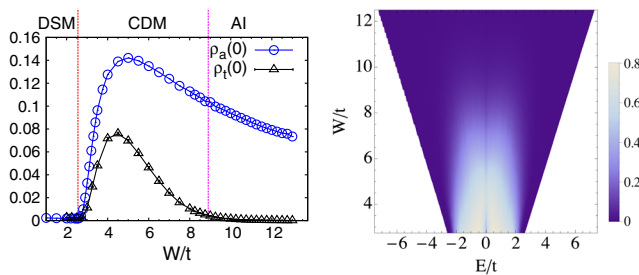
possible (DSM-CDM-AI) QPTs (see Fig. 1). We firmly establish that a disordered DSM in three dimensions possesses two distinct QPTs as a function of disorder strength, as shown in Figs. 1 and 3. The TDOS at zero energy is only finite in the CDM region $W_c < W < W_l$, in contrast to the ADOS at zero energy which is finite for any $W > W_c$. This provides unambiguous evidence for the existence of three phases and the different nature of the two distinct disorder-tuned QPTs. The nature of the QCP between the DSM and the CDM phases has been studied through an extensive numerical computation of the ADOS in Refs. [32,34]. As the TDOS and the ADOS track each other in a metal, our calculation provides further numerical evidence for the stability of the DSM phase in the presence of weak disorder. We supplement the DOS analysis through exact calculations of the wave function for small system sizes in order to estimate the critical exponents of the Anderson localization transition. Here, our goal is not to establish the precise values for the critical exponents of the Anderson localization transition. Rather, we want to show that the estimated critical exponents for the CDM-AI QCP are comparable to the ones known for the conventional orthogonal (AI) Wigner-Dyson universality class [17,19], and are strikingly different from the ones obtained for the DSM-CDM QCP [32,34]. Since our model of a DSM preserves time reversal symmetry, we expect the Anderson localization transition to be described by the orthogonal (AI) class [17,19,37] for short range disorder.

We consider the following Hamiltonian on a cubic lattice with periodic boundary conditions:

$$H = \frac{1}{2} \sum_{\mathbf{r},\hat{\mu}} (it\psi_{\mathbf{r}}^{\dagger}\alpha_{\mu}\psi_{\mathbf{r}+\mathbf{e}_{\hat{\mu}}} + H.c.) + \sum_{\mathbf{r}} V(\mathbf{r})\psi_{\mathbf{r}}^{\dagger}A_{W}\psi_{\mathbf{r}},$$

(1)

where $\psi_{\mathbf{r}}^{T} = (c_{\mathbf{r},+,\uparrow}, c_{\mathbf{r},-,\uparrow}, c_{\mathbf{r},+,\downarrow}, c_{\mathbf{r},-,\downarrow})$ is a four component Dirac spinor composed of an electron at site $\mathbf{r}$, with a

FIG. 1 (color online). Phase diagram of three dimensional Dirac semimetals. Left: $\rho_a(0)$ and $\rho_t(0)$ for $L = 60$, clearly displaying the existence of three distinct phases DSM, CDM, and AI. The TDOS tracks the ADOS inside the DSM, through the semimetal-metal QCP, and then $\rho_t(0)$ goes to zero at W_l, signaling the Anderson localization transition. Right: $M_{\text{edge}}(E)$ as a function of energy and disorder strength for $L = 60$. The white and the blue regions are, respectively, metallic and localized, and the blank region is gapped (outside the bandwidth), which clearly shows the existence of the energy dependent mobility edge. The value of $M_{\text{edge}}(E)$ is shown in the key.
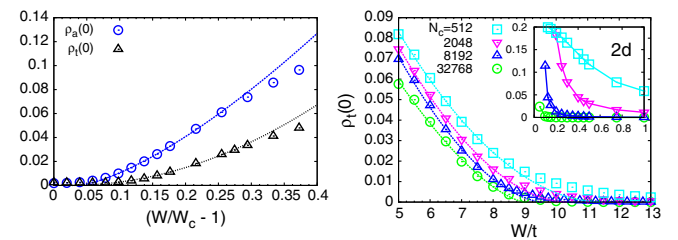

FIG. 2 (color online). Critical properties of the two quantum critical points. Left: power law dependence of $\rho_a(0)$ and $\rho_t(0)$ as a function of disorder strength in the vicinity of the DSM-CDM QCP for $L = 60$. Right: the Anderson localization QCP from the TDOS as a function of the Chebyshev expansion order N_c for $L = 30$, respectively, in three and (inset) two dimensions. We find the localization transition in three dimensions is converging to $W_l^{3d}/t = 8.9 \pm 0.3$ in three dimensions whereas in two dimensions $W_l^{2d}/t \to 0$ as $N_c \to \infty$ by extrapolating $\rho_t(0)$ to zero (dashed lines).
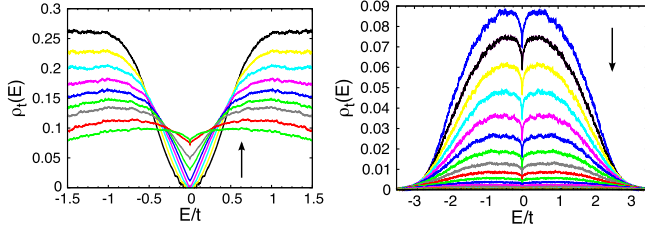
FIG. 3 (color online). TDOS with $L = 60$ as a function of energy for various values of disorder. Left: passing through the DSM-CDM QCP, Right: passing through the Anderson localization transition. The arrows denote increasing disorder strengths from $W/t = 2.0$ to 4.5 (left) and from $W/t = 5.0$ to 13.0 (right). We see no signs of rare region effects [35] in the numerics.

parity ($\pm$) and spin ($\uparrow/\downarrow$), $\hat{\mu} = \hat{x}, \hat{y}, \hat{z}$, $\mathbf{e}_{\hat{\mu}}$ is a unit vector that points to each nearest neighbor, and the α_μ are 4×4 anticommuting Dirac matrices. In the absence of disorder, the tight binding model gives rise to eight Dirac cones at the Γ, M, R, and X points of the cubic Brillouin zone. The disorder potential at each site $V(\mathbf{r})$ is a randomly distributed variable between $[-W/2, W/2]$ and A_W is a matrix that specifies the type of disorder. We primarily focus on the random axial chemical potential $A_W = \gamma_5 = i\alpha_1\alpha_2\alpha_3$, but also discuss the effects of a random scalar potential $A_W = I_{4\times4}$ (where $I_{4\times4}$ is a four by four identity matrix). We consider these two types of disorder because we want to demonstrate universality in the sense that both disorders give rise to identical phase diagrams. This is also implied by the existence of two continuous U(1) symmetries under $\psi \to e^{i\theta}\psi$ and $\psi \to e^{i\phi\gamma_5}\psi$. In addition, axial disorder is pertinent for addressing the phase diagram of dirty gapless superconductors.

TDOS and ADOS.—To track the nature of each phase of the model defined in Eq. (1), we first calculate the ADOS, the local DOS (LDOS), and the TDOS using the KPM (see Ref. [36] for details), which are defined as

$$\rho_a(E) = \left\langle \frac{1}{4V} \sum_{i=1}^{V} \sum_{\alpha=1}^{4} \delta(E - E_{i\alpha}) \right\rangle, \qquad (2)$$

$$\rho_{i\alpha}(E) = \sum_{k,\beta} |\langle k, \beta | i, \alpha \rangle|^2 \delta(E - E_{k\beta}), \qquad (3)$$

$$\rho_t(E) = \exp\left(\frac{1}{4N_s} \sum_{i=1}^{N_s} \sum_{\alpha=1}^{4} \langle \log \rho_{i\alpha}(E) \rangle \right). \qquad (4)$$

The size of the system considered is $V = L^3$, where $|i, \alpha\rangle$ denotes an eigenstate at site i and orbital α (one of the four Dirac orbitals) with an energy $E_{i\alpha}$, and the $\langle \ldots \rangle$ denotes a disorder average. As the ADOS is self-averaging, we only include the disorder average to smoothen the data. For the calculations of the ADOS presented here with a system size $V = 60^3$ we have only used 12 disorder averages. In

contrast, the TDOS is not a self-averaging quantity and it requires a significant number of disorder averages to obtain a convergent result. After the disorder averaging, translation symmetry is restored and consequently we also sum over a finite number of lattice sites $N_s \ll V$ to improve the statistics. We provide the parameters used in the study in the Supplemental Material [37]. Central to the KPM, we first expand the LDOS or the ADOS in terms of the orthogonal Chebyshev polynomials up to an order N_c. For the ADOS we have considered $N_c = 1028$, whereas the computation of the TDOS is much more demanding [36] and for most of the calculations we have used $N_c = 8192$, unless stated otherwise.

The DSM is characterized by an ADOS $\rho_a(E) \propto |E|^2$, that vanishes at zero energy. As shown in Fig. 1, both $\rho_a(0)$ and $\rho_t(0)$ vanish for weak disorder strengths, and concomitantly become finite after passing through the DSM-CDM QCP at $W_c/t \approx 2.55$ [34], in a power law fashion as

$$\rho_a(E = 0, W \geq W_c) \sim (W - W_c)^x, \qquad (5)$$

$$\rho_t(E = 0, W \geq W_c) \sim (W - W_c)^{x_t}, \qquad (6)$$

where we find $x = 1.4 \pm 0.2$ (in agreement with Refs. [32,34] for much larger system sizes) and $x_t = 2.0 \pm 0.3$ as shown in Fig. 1. Physically, the average moments of the LDOS $\langle \rho_i(E)^n \rangle$ captures the multifractal nature of the disordered wave function [17,18,42]. Therefore the difference $x_t - x = 0.60 \pm 0.36$ reveals the underlying multifractal nature of the DSM-CDM QCP. We have checked that the value of W_c determined from $\rho_a(0)$ is within numerical accuracy unaffected by increasing N_c.

Inside the CDM phase $\rho_t(0)$ tracks $\rho_a(0)$ ($\rho_t \sim \rho_a$) up to $W/t \approx 4.5$. As ρ_a is a *self-averaging* quantity, we can conclude that the DSM-CDM transition is completely independent of Anderson localization. For larger values of disorder ($W/t > 4.5$) ρ_a remains finite and ρ_t goes to zero continuously at the localization transition as

$$\rho_t(E = 0, W \leq W_l) \sim (W_l - W)^\beta. \qquad (7)$$

We determine the location of the transition by studying the effect of increasing the Chebyshev expansion order on ρ_t, as W_l has been shown to be sensitive to N_c in Ref. [43]. By extrapolating $\rho_t(E = 0)$ to zero, we find $W_l/t = 8.9 \pm 0.3$ with an order parameter critical exponent $\beta = 1.5 \pm 0.2$, as shown in Fig. 2.

In order to further understand the stability of the CDM against localization effects, we compare the TDOS for a DSM in two and three spatial dimensions in Fig. 2. The two dimensional model of a DSM is obtained by setting the hopping along the z direction to zero in Eq. (1), which gives rise to four Dirac cones at the high symmetry points of the Brillouin zone for a square lattice. In two dimensions, both axial and scalar potential disorders are marginally relevant

perturbations, and an infinitesimal amount of disorder leads to an AI [37,44,45]. This is in excellent agreement with our numerical results, namely, $W_l^{2d}/t \to 0$ as $N_c \to \infty$. In contrast, in three dimensions we find the DSM phase to be stable up to W_c (Fig. 1), where $\rho_a(0)$ and $\rho_t(0)$ simultaneously develop finite values, and the CDM phase undergoes an Anderson localization at a much larger disorder strength W_l. Therefore, our results establish the existence of three distinct ground states for a dirty DSM in three dimensions (DSM/CDM/AI with increasing disorder), in agreement with the field theoretic analysis.

By considering the energy dependence of ρ_t as shown in Fig. 3, we find $\rho_t(E) \sim |E|^2$ inside the DSM phase [i.e., in agreement with $\rho_a(E)$ [37]]. In contrast, $\rho_t(0)$ approaches a constant inside the CDM phase. Within this framework, we can capture the location of the mobility edge separating the CDM and AI phases by considering the ratio $M_{\mathrm{edge}}(E) = \rho_t(E)/\rho_a(E)$. As shown in Fig. 1, starting from the CDM phase, the system develops a finite, energy dependent mobility edge and the entire band localizes for a larger disorder strength going to an AI phase, qualitatively similar to the situation for a three dimensional CM. Because of the underlying Dirac band structure, the shape of the mobility edge is different from a conventional tight binding model (e.g., see Ref. [46]). This phase diagram also demonstrates that a DSM away from half-filling behaves as a CM.

Wave function.—In order to understand the critical properties of the localization transition and compare our results with the well-established universality classes for Anderson localization, we now study the properties of the wave function. The qualitative nature of the wave function also displays all of the physics we have discussed so far [37]. Here, we focus on the average participation ratio defined as

$$P_{\mathrm{avg}} = \left\langle \frac{[\sum_{i,\alpha}|\psi_\alpha(\mathbf{r}_i)|^2]^2}{\sum_{i,\alpha}|\psi_\alpha(\mathbf{r}_i)|^4} \right\rangle \quad (8)$$

for wave functions $\psi_\alpha(\mathbf{r}_i)$ and only focus on the center of the band $E = 0$ (otherwise P_{avg}^{-1} will be a function of energy). It is well known [18] that the IPR scales as $P_{\mathrm{avg}}^{-1} \sim 1/V$ in a metallic phase and $P_{\mathrm{avg}}^{-1} \sim$ const in a localized phase [37]. As these calculations require an exact diagonalization of the Hamiltonian, we are restricted to much smaller lattice sizes than considered for the DOS. Here we focus on linear system sizes $L = 4, 6, 8, 10, 12$ with 10 000 disorder realizations for $L = 4$–10 and 1000 for $L = 12$. Because of the limited system sizes, we first expand the IPR in the vicinity of the localization transition in terms of an unknown scaling function f and L dependent corrections, [18,46–49] $P_{\mathrm{avg}}^{-1} \approx L^{-d_2}[f((1 - W_l/W)L^{1/\nu}) + A_0/L^y]$. We have introduced the fractal dimension d_2, the localization
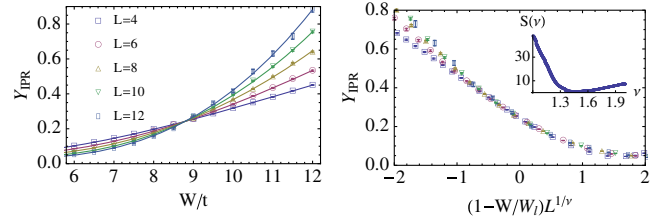

FIG. 4 (color online). Finite size scaling of the IPR. Left: determining the location of the Anderson localization transition by optimizing the crossing location of Y_{IPR} by third order polynomial fits to the IPR; this yields $W_l/t = 8.8 \pm 0.3$. Right: data collapse of Y_{IPR} in the vicinity of W_l as a function of $(1 - W_l/W)L^{1/\nu}$, yields a localization length exponent $\nu = 1.5 \pm 0.2$. Inset: optimizing the data collapse using the local linearity function $S(\nu)$ (as described in Ref. [51]); the value of ν is determined by the minimum of $S(\nu)$.

length exponent ν, A_0 is a finite size correction, and y the leading order irrelevant variable's critical exponent [47]. To determine the location of the transition we calculate the best recursive fit to $Y_{\mathrm{IPR}} = P_{\mathrm{avg}}^{-1}L^{d_2} - A_0 L^{-y}$, using finite size scaling techniques [47,50]; see Fig. 4. As a result, we find a localization transition at $W_l/t = 8.8 \pm 0.3$ in excellent agreement with the typical DOS results. This also yields $d_2 = 1.2 \pm 0.3$, $y = 2.3 \pm 0.5$, and $A_0 = 1.8 \pm 0.6$.

Now that we have determined the critical point using two different methods we perform scaling data collapse to extract the localization length exponent, which yields $\nu = 1.5 \pm 0.2$. Within the numerical accuracy, ν, y, and d_2 are consistent with the known exponents for the orthogonal (AI) class ($\nu = 1.57$, $y = 2.8$, and $d_2 = 1.23$) [46,47,52]. In previous studies of Anderson localization, it was found that typical DOS exponent satisfies $\beta = \nu(\alpha_0 - d)$ [18,19]. We also find this relation to hold with $\alpha_0 = 4.0 \pm 0.3$, which is consistent with $\alpha_0 = 4.043$ [52] for class AI.

In conclusion, we have performed a detailed numerically exact study of the quantum phase diagram and Anderson localization in three dimensional dirty DSMs. By studying the TDOS on sufficiently large lattices we have established the existence of three phases for a half-filled system DSM, CDM and AI, separated by two different QCPs as a function of disorder. We have supplemented this with a precise finite size scaling analysis of the IPR and obtained the critical exponents of the localization transition. We also establish clear signatures for multifractility at the QPTs. In addition, we find the localization properties for both axial and scalar potential disorders to be identical (to within numerically accuracy) [37], and therefore, we conclude that the QPTs driven by either disorder belong to the same universality class. As the model we have studied for axial or potential disorder separates into two blocks of Weyl Hamiltonians [37], our results are equally valid for three dimensional time reversal symmetric Weyl systems.

[1] P. A. Dirac, Proc. R. Soc. A **117**, 610 (1928).

[2] R. Dornhaus, G. Nimtz, and B. Schlicht, *Narrow-Gap Semiconductors* (Springer, New York, 1983).

[3] M. Neupane, S.-Y. Xu, R. Sankar, N. Alidoust, G. Bian, C. Liu, I. Belopolski, T.-R. Chang, H.-T. Jeng, H. Lin *et al.*, Nat. Commun. **5**, 3786 (2014).

[4] Z. Liu, J. Jiang, B. Zhou, Z. Wang, Y. Zhang, H. Weng, D. Prabhakaran, S. Mo, H. Peng, P. Dudin *et al.*, Nat. Mater. **13**, 677 (2014).

[5] S. Borisenko, Q. Gibson, D. Evtushinsky, V. Zabolotnyy, B. Büchner, and R. J. Cava, Phys. Rev. Lett. **113**, 027603 (2014).

[6] S.-Y. Xu, C. Liu, S. K. Kushwaha, R. Sankar, J. W. Krizan, I. Belopolski, M. Neupane, G. Bian, N. Alidoust, T.-R. Chang *et al.*, Science **347**, 294 (2015).

[7] B. Lenoir, M. Cassart, J.-P. Michenaud, H. Scherrer, and S. Scherrer, J. Phys. Chem. Solids **57**, 89 (1996).

[8] A. Ghosal, P. Goswami, and S. Chakravarty, Phys. Rev. B **75**, 115123 (2007).

[9] J. C. Y. Teo, L. Fu, and C. L. Kane, Phys. Rev. B **78**, 045426 (2008).

[10] S.-Y. Xu, Y. Xia, L. Wray, S. Jia, F. Meier, J. Dil, J. Osterwalder, B. Slomski, A. Bansil, H. Lin *et al.*, Science **332**, 560 (2011).

[11] T. Sato, K. Segawa, K. Kosaka, S. Souma, K. Nakayama, K. Eto, T. Minami, Y. Ando, and T. Takahashi, Nat. Phys. **7**, 840 (2011).

[12] M. Brahlek, N. Bansal, N. Koirala, S.-Y. Xu, M. Neupane, C. Liu, M. Z. Hasan, and S. Oh, Phys. Rev. Lett. **109**, 186403 (2012).

[13] L. Wu, M. Brahlek, R. V. Aguilar, A. Stier, C. Morris, Y. Lubashevsky, L. Bilbro, N. Bansal, S. Oh, and N. Armitage, Nat. Phys. **9**, 410 (2013).

[14] S.-Y. Xu, C. Liu, N. Alidoust, M. Neupane, D. Qian, I. Belopolski, J. Denlinger, Y. Wang, H. Lin, L. Wray *et al.*, Nat. Commun. **3**, 1192 (2012).

[15] Q. D. Gibson, L. M. Schoop, L. Muechler, L. S. Xie, M. Hirschberger, N. P. Ong, R. Car, and R. J. Cava, Phys. Rev. B **91**, 205128 (2015).

[16] P. A. Lee and T. V. Ramakrishnan, Rev. Mod. Phys. **57**, 287 (1985).

[17] D. Belitz and T. R. Kirkpatrick, Rev. Mod. Phys. **66**, 261 (1994).

[18] M. Janssen, Phys. Rep. **295**, 1 (1998).

[19] F. Evers and A. D. Mirlin, Rev. Mod. Phys. **80**, 1355 (2008).

[20] P. W. Anderson, Phys. Rev. **109**, 1492 (1958).

[21] E. Abrahams, P. W. Anderson, D. C. Licciardello, and T. V. Ramakrishnan, Phys. Rev. Lett. **42**, 673 (1979).

[22] R. Bell and P. Dean, Discuss. Faraday Soc. **50**, 55 (1970).

[23] F. Wegner, Z. Phys. B: Condens. Matter **36**, 209 (1980).

[24] V. Dobrosavljević, A. Pastor, and B. Nikolić, Europhys. Lett. **62**, 76 (2003).

[25] G. Schubert, J. Schleede, K. Byczuk, H. Fehske, and D. Vollhardt, Phys. Rev. B **81**, 155106 (2010).

[26] E. Fradkin, Phys. Rev. B **33**, 3263 (1986).

[27] P. Goswami and S. Chakravarty, Phys. Rev. Lett. **107**, 196803 (2011).

[28] Y. Ominato and M. Koshino, Phys. Rev. B **89**, 054202 (2014).

[29] B. Roy and S. Das Sarma, Phys. Rev. B **90**, 241112 (2014).

[30] S. V. Syzranov, V. Gurarie, and L. Radzihovsky, Phys. Rev. B **91**, 035133 (2015).

[31] S. V. Syzranov, L. Radzihovsky, and V. Gurarie, Phys. Rev. Lett. **114**, 166601 (2015).

[32] K. Kobayashi, T. Ohtsuki, K.-I. Imura, and I. F. Herbut, Phys. Rev. Lett. **112**, 016402 (2014).

[33] B. Sbierski, G. Pohl, E. J. Bergholtz, and P. W. Brouwer, Phys. Rev. Lett. **113**, 026602 (2014).

[34] J. H. Pixley, P. Goswami, and S. Das Sarma, arXiv: 1505.07938.

[35] R. Nandkishore, D. A. Huse, and S. L. Sondhi, Phys. Rev. B **89**, 245110 (2014).

[36] A. Weiße, G. Wellein, A. Alvermann, and H. Fehske, Rev. Mod. Phys. **78**, 275 (2006).

[37] See Supplementary Material at http://link.aps.org/supplemental/10.1103/PhysRevLett.115.076601, which includes Refs. [38–41], for a discussion of the field theory and additional numerical results.

[38] P. Goswami and S. Tewari, Phys. Rev. B **88**, 245107 (2013).

[39] S. Hikami, Phys. Lett. **98B**, 208 (1981).

[40] F. Wegner, Nucl. Phys. **B316**, 663 (1989).

[41] S. Hikami, Prog. Theor. Phys. Suppl. **107**, 213 (1992).

[42] M. S. Foster, Phys. Rev. B **85**, 085122 (2012).

[43] G. Schubert, A. Weiße, G. Wellein, and H. Fehske, in *High Performance Computing in Science and Engineering, Garching 2004* (Springer, New York, 2005), pp. 237–249.

[44] I. L. Aleiner and K. B. Efetov, Phys. Rev. Lett. **97**, 236801 (2006).

[45] A. Altland, Phys. Rev. Lett. **97**, 236802 (2006).

[46] J. Brndiar and P. Markoš, Phys. Rev. B **74**, 153103 (2006).

[47] K. Slevin and T. Ohtsuki, Phys. Rev. Lett. **82**, 382 (1999).

[48] A. D. Mirlin, Phys. Rep. **326**, 259 (2000).

[49] A. Mildenberger, F. Evers, and A. D. Mirlin, Phys. Rev. B **66**, 033109 (2002).

[50] N. C. Murphy, R. Wortis, and W. A. Atkinson, Phys. Rev. B **83**, 184206 (2011).

[51] N. Kawashima and N. Ito, J. Phys. Soc. Jpn. **62**, 435 (1993).

[52] L. Ujfalusi and I. Varga, Phys. Rev. B **91**, 184206 (2015).